Supporting Information

Effects of Lanthanide Doping on the Catalytic Activity and Hydrothermal Stability of Cu-SAPO-18 Catalysts for the catalytic removal of NO_x (NH_3-SCR) from diesel engines

Qi Gao[a], Shuai Han[a], Qing Ye[a,*], Shuiyuan Cheng[a], Tianfang Kang[a], Hongxing Dai[b,*]

[a] Key Laboratory of Beijing on Regional Air Pollution Control, Department of Environmental Science, College of Environmental and Energy Engineering, Beijing University of Technology, Beijing 100124, China

[b] Beijing Key Laboratory for Green Catalysis and Separation, Key Laboratory of Beijing on Regional Air Pollution Control, and Laboratory of Catalysis Chemistry and Nanoscience, Department of Chemistry and Chemical Engineering, College of Environmental and Energy Engineering, Beijing University of Technology, Beijing 100124, China

* Corresponding authors:

Prof. Qing Ye: Tel. No.: +8610 6739 1659; Fax: +8610 6739 1983; E-mail address: yeqing@bjut.edu.cn (Q. Ye)

Prof. Hongxing Dai: Tel.: +8610 6739 6118; Fax: +8610 6739 1983; E-mail: hxdai@bjut.edu.cn (H. Dai)

1. Catalyst preparation procedures:

The SAPO-18 zeolite was synthesized using N,N-diisopropyle-thylamine ($C_8H_{19}N$, DIPEA) as structure-directing agent. The composition of Al_2O_3 : P_2O_5: SiO_2 : DIPEA : H_2O in molar ratio was 1.0 : 0.9 : 0.3 : 2.0 : 50. The gel was sealed in a Teflon-lined stainless steel autoclave and heated at 170 °C for 8 days. The obtained mixture was washed with deionized water and filtered. After being dried at 120 °C overnight, the dried powders were calcined in air at 550 °C for 12 h to remove the organics, thus obtaining the SAPO-18 zeolite.

The SAPO-18 zeolite was further ion-exchanged with a NH_4Cl aqueous solution (0.1 mol/L) at 75 °C for 8 h under stirring to form NH_4/SAPO-18 (1.0 g of SAPO-18 was dispersed in 60 mL of the NH_4Cl aqueous solution) [1]. The solution is in turn filtered, washed with deionized water (until no Cl^- ions were detected), and dried at 120 °C for 12 h. Afterwards, 1.0 g of NH_4/SAPO-18 was added to 60 mL of the mixed solution containing the desired amount of $Cu(NO_3)_2$ and $M(NO_3)_3$ (M = La, Ce, Nd, Gd, Tb, Ho or Lu), in which 30 mL of $Cu(NO_3)_2$ aqueous solution (0.05 mol/L) was added to 30 mL of $M(NO_3)_3$ aqueous solution (0.0075 mol/L) at 60 °C for 4 h under stirring. Then, the samples were dried in a dry oven at 120 °C for 12 h to remove residual water. After being calcined in an air flow (30 mL) at 500 °C for 6 h (The Cu-SAPO-18 and Ce-Cu-SAPO-18 samples were calcined at 500 and 600 ^oC, respectively, and their activities for the NH_3-SCR reaction were evaluated. It is found that there was no significant change in their NH_3-SCR activity even though the

calcination temperature reached 600 ^{o}C, as shown in Fig. S1. Therefore, 500 ^{o}C was chosen as the calcination temperature.), the obtained samples were denoted as M-Cu-SAPO-18 (called as the fresh samples). It should be pointed out that these M-Cu-SAPO-18 samples contained a similar actual copper loading of 1.76 ± 0.2 wt % (measured by the XRF technique). In order to examine the hydrothermal stability, the M-Cu-SAPO-18 samples were first treated in a 10 % H_2O-containing air flow (300 mL/min) at a ramp of 10 °C/min from 30 to 850 °C, and then kept at the corresponding final temperature for 12 h. The above treated samples were called as the hydrothermally aged samples.

2. Catalyst characterization

The crystal structures of the samples were determined on an X-ray diffractometer (XRD, X'Pert-Pro MPD, Philips, Netherlands) using the CuKα radiation, and the diffraction angle was in the range of 5 ~ 50° at a scanning speed of 5°/min. The Cu contents in the samples were analyzed using an X-ray fluorescence spectrometer (XRF-1800, Shimadzu). X-ray photoelectron spectroscopy (XPS) was used to determine the surface O, Ce, and Cu species concentrations on an ESCALAB 250Xi spectrometer (Thermo Fisher, U.S.) using an AlKα (hv = 1486.5 eV) radiation source. H_2 temperature-programmed reduction (H_2-TPR) of the samples was carried out on the Builder PCA-1200 analyzer. Prior to H_2-TPR experiment, 100 mg of the sample was pretreated in a 5 vol% O_2/N_2 mixture flow of 30 mL/min at 400 °C for 1 h, and subsequently cooled to room temperature (RT). The sample was then reduced in a 5 vol%

H_2/N_2 mixture flow of 30 mL/min at a ramp of 10 °C/min from RT to 1000 °C. Nuclear magnetic resonance (NMR) spectra of the samples were measured on an Avance III HD 500NMR spectrometer. The ^{27}Al magic angle spinning NMR spectra of the samples were recorded at a resonance frequency of 156.26 MHz. The ^{27}Al chemical shifts were reported to be related to 0.1 mol/L $Al(NO_3)_3$ aqueous solution. Ammonia temperature-programmed desorption (NH_3-TPD) of the samples was conducted on the Builder PCA-1200 analyzer. The sample (100 mg) was pretreated at 500 °C and saturated with NH_3 (30 mL/min) at 100 °C. After being purged with pure He (30 mL/min) at 100 °C for 1 h, NH_3 desorption took place in a He flow of 30 mL/min at a ramp of 10 °C/min and the temperature range of 30 ~ 850 °C. The in situ DRIFTS experiments were carried out on a Bruker TENSOR II spectrometer with a reaction chamber that could withstand high temperatures (Harrick Praying Mantis). For each of the in situ DRIFTS experiments, the sample (60 mg) was placed into the sample cup of the reaction chamber. Before being cooled to 30 °C, the sample was pretreated at 550 °C in a 5 vol% O_2/N_2 flow of 100 mL/min for 0.5 h. For the NH_3 adsorption experiments, the sample was exposed to a 500 ppm NH_3/N_2 flow of 100 mL/min. The NH_3 adsorption spectrum of each sample was obtained by subtracting the background spectrum that was recorded by exposing the sample to a pure N_2 flow of 100 mL/min.

3. Catalytic Evaluation

Catalytic activity was evaluated using a quartz tubular fixed-bed microreactor. The NH_3-SCR reactions were carried out in the microreactor by mixing 150 mg of the catalyst with 150 mg of quartz sands. The simulated exhaust gas was composed of 500 ppm NO + 500 ppm NH_3 + 14 vol% O_2 + 5 vol% H_2O + N_2 (balance). The total gas flow rate was 300 mL/min and the gas hourly space velocity (GHSV) was about 66,000 h^{-1}. The concentration of NO, NO_2, N_2O was measured on the Bruker TENSOR II spectrometer with 1.5 m of a heating cell.

The NH_3 oxidation reactions were carried out in a microreactor by mixing 150 mg of the catalyst with 150 mg of quartz sands. The simulated exhaust gas was composed of 500 ppm NH_3 + 14 vol% O_2 + 5 vol% H_2O + N_2 (balance). The total gas flow rate was 300 mL/min and the gas hourly space velocity (GHSV) is about 66,000 h^{-1}. The effluent NH_3 concentration was measured on the Bruker TENSOR II spectrometer with 1.5 m of a heating cell. All of the gas lines in the reaction system were heated to 150 °C to prevent the possible water condensation.

The NO conversions, NH_3 conversions, and N_2 selectivity were calculated according to their inlet ($[NO]_{inlet}$, and $[NH_3]_{inlet}$) and outlet ($[NO]_{outlet}$, $[NO_2]_{outlet}$, $[N_2O]_{outlet}$, and $[NH_3]_{outlet}$) concentrations at a steady state, as shown in Eqs. (S1), (S2) and (S3):

$$\text{NO conversions (\%)} = \frac{[NO]_{inlet} - [NO + NO_2 + N_2O]_{outlet}}{[NO]_{inlet}} \times 100\% \quad \text{(S1)}$$

$$NH_3 \text{ conversion } (\%) = \frac{[NH_3]_{inlet} - [NH_3]_{outlet}}{[NH_3]_{inlet}} \times 100\% \quad \text{(S2)}$$

$$N_2 \text{ selectivity } (\%) = \left(1 - \frac{2[N_2O]_{outlet}}{[NO]_{inlet} + [NH_3]_{inlet} - [NO]_{outlet} - [NO_2]_{outlet} - [NH_3]_{outlet}}\right) \times 100\% \quad \text{(S3)}$$

The NH_3-SCR kinetic measurements over the catalysts were carried out in a plug-flow microreactor, and the outlet NO concentrations were analyzed by a Thermo Model 42i-HL analyser. The GHSV was about 400,000 h^{-1}. Under the adopted reaction conditions, the diffusion effects were eliminated. 25 mg of the sample well mixed with 125 mg of quartz sands was placed in the differential reactor. The typical time to achieve a steady state at a given temperature was 1 h. The NH_3-SCR reaction rate (r (molNO/(gcat s))), which was defined as the number of NO molecules converted per second over the catalyst, were calculated according to Eq. (S4):

$$r = \frac{X_{NO} \times F_{NO}}{m_{cat} \times 60 \times 22.4} \quad \text{(S4)}$$

where X_{NO} (%) is the NO conversion, F_{NO} (L/min) is the volumetric NO flow rate, and mcat (g) is the catalyst mass.

4. Discussion

It has been known that the doping of lanthanide elements has an impact on the NH_3-SCR reaction of the Cu-containing zeolite catalysts. According to the literature [40], the co-doping of Cu and other metals may play the roles as follows: (i) directly participating the reaction mechanism, (ii) changing the electrostatic field and surface potential in zeolite pores or cavities, (iii) changing the local softness of copper ions, (iv) modification of copper complexes and/or mobility, and (v) changing in NO diffusion

characteristics [41]. Actually, the roles of these doped metals are difficult to be identified. We try to explain the roles of M-doping in enhancing the catalytic activities and hydrothermal stability of the M-Cu-SAPO-18 samples, as discussed below.

4.1 Analysis of the Properties of M-Cu-SAPO-18 Catalysts

Based on the results of the sample characterization and NH_3-SCR activity evaluation, we can realize that the catalytic activities of the M-Cu-SAPO-18 samples were related to their structure, reducibility, active Cu species, and acid sites. The NH_3-SCR reaction took place on the surface active centers. A larger specific surface area can provide a more amount of active sites, which increases the contacting opportunity between the reactants and the surface active centers of the catalyst and thus accelerate the NH_3-SCR reaction. The surface areas of M-Cu-SAPO-18 were lower than that of Cu-SAPO-18, a result possibly due to the blocking of partial zeolite cavities by the CuO_x and MO_x entities. Hence, the pore volumes and surface areas decreased, as evidenced by the results of BET measurements (Table 1). Among all of the fresh M-Cu-SAPO-18 samples, Ce-Cu-SAPO-18 showed the largest surface area. Although the surface area of Ce-Cu-SAPO-18 was lower than that of Cu-SAPO-18, the NH_3-SCR activity over the former was higher than that over the latter. This result demonstrates that the surface area was not the only factor determining the catalytic activity. The amount and distribution of the isolated Cu^{2+} species directly influenced the catalytic activity of the sample. From the H_2-TPR results, the reduction peak (α) at the lower temperature was assigned to the reduction of the isolated Cu^{2+} ions in the 8MRs cage, which is related to the reaction of the catalyst SCR at low temperature, and The

reduction peak (γ) at the higher temperature was attributed to the reduction of Cu^{2+} ions in the D6R cage, which is closely related to the activity of middle and high temperature range. In the fresh Cu-SAPO-18 sample, a more amount of the isolated Cu^{2+} species was likely to reside within the 8MRs cage, which is the cause of good low temperature NH_3-SCR activity of Cu-SAPO-18 catalyst (Figure 1). After the doping of lanthanide elements, the distribution of the isolated Cu^{2+} species was accordingly changed, as compared with the Cu-SAPO-18 sample. The co-doping of Cu and M could influence the amount of the isolated Cu^{2+} species in the D6R cage (the most stable sites and the active sites of middle and high temperature range), as evidenced indirectly by the H_2-TPR results (Figure 8 and Table 3). For the Ho-, Tb- or Lu-doped Cu-SAPO-18 sample, the amount of the isolated Cu^{2+} species decreased but the amount of the CuO_x species increased, as compared with the Cu-SAPO-18 sample. It is conceivable that the co-doping of Cu and M preferred to dwell at the 8MRs cage and prevented the Cu^{2+} ions from migrating to the most stable sites (the D6R cage), which induced the accumulation of the aggreged CuO_x during calcination. Additionally, the amount of the total isolated Cu^{2+} species in the Ce-Cu-SAPO-18 sample was more than that in the other M-Cu-SAPO-18 samples. More importantly, the amount of the isolated Cu^{2+} species in the D6R cage of the Ce-Cu-SAPO-18 sample significantly increased, as compared with the fresh Cu-SAPO-18 sample. These results suggest that the doping of Ce enhanced not only the dispersion of Cu species in the sample, but also strengthened the interaction between the isolated Cu^{2+} species and zeolitic framework. From the results of Cu $2p_{3/2}$ XPS (Figure 6), the amount of surface isolated Cu^{2+} species on Ce-Cu-SAPO-18

increased more markedly than those on the other M-Cu-SAPO-18 samples. A more amount of Cu^{2+} ions was stabilized in the D6R cage, inducing a band at 895 cm^{-1} of tetrahedral cation-oxygen-tetrahedral cation (T−O−T) framework (as clearly shown in DRIFTS-NH_3 adsorption (Figure 11)). In conclusion, the highest amount and best distribution of the isolated Cu^{2+} species were responsible for the best catalytic activity (Figure 1) of the Ce-Cu-SAPO-18 sample.

4.2 Effect of Lanthanide Doping on Hydrothermal Stability

The Cu-SAPO-18 and M-Cu-SAPO-18 samples showed different responses to the hydrothermal aging treatment. It has long been recognized that the effect of hydrothermal aging treatment on the microporous zeolitic structure can be clarified by the XRD, ^{27}Al MAS NMR, and N_2 sorption measurements. The doping of lanthanide elements induced different changes in zeolitic structure of Cu-SAPO-18. After the addition of Tb, the zeolite skeleton partially destroyed after the hydrothermal aging treatment, so the hydrothermal stability of the Tb-Cu-SAPO-18 sample was poor. In particular, the worst decreases in surface area and micropore volume occurred after the hydrothermal aging treatment due to the presence of CuO aggregates that partial clogging or filled the pores, which were proven by the H_2-TPR and BET results (Figure 9, Table 1, and Table 3). The hydrothermal stability decreased in the order of Ce-Cu-SAPO-18-aged > Gd-Cu-SAPO-18-aged > La-Cu-SAPO-18-aged > Nd-Cu-SAPO-18-aged > Cu-SAPO-18-aged > Ho-Cu-SAPO-18-aged > Tb-Cu-SAPO-18-aged > Lu-Cu-SAPO-18-aged, which was in good agreement with the H_2-TPR results of the total

isolated Cu^{2+}(Table 3 and Figure 9). Additionally, as clearly seen from the XRD patterns (Figure 5), the crystal structure of Ce-Cu-SAPO-18 did not change significantly after the hydrothermal aging treatment, still maintaining a good crystallinity. In addition, no additional diffraction peaks indicate that no new crystalline phase is formed, suggesting that the Cu and Ce were well dispersed within the SAPO-18 zeolite after the hydrothermal aging treatment (Figure 5). Similarly, the ^{27}Al MAS NMR spectra of the Ce-Cu-SAPO-18 sample also reveal no significant framework dealumination after the hydrothermal aging treatment. For the Ce-Cu-SAPO-18-aged sample, only a small decrease (4.1 %) in resonance intensity of the tetrahedral Al was observed, as compared with the fresh sample. The structure of 8MRs in SAPO-18 was unstable and easy to hydrolyze, but the doping of Cu and M could inhibit the hydrolysis of the 8MRs cage. According to the above results, the Ce-doped Cu-SAPO-18 sample possessed the strongest ability to prevent the hydrolysis, while the Lu-doped Cu-SAPO-18 sample was the least effective. This trend was qualitatively consistent with the change in acidic sites of the fresh and hydrothermally aged samples, as observed from the NH_3-TPD and in situ DRIFTS-NH_3 adsorption (Figures 11−13). Therefore, it can be concluded that the co-doping of Cu and M could protect the zeolite from hydrolyzing during the hydrothermal aging treatment process by decreasing the density of the most vulnerable acidic −Si−(OH)−Al− sites. More attention should be paid to the change in Cu species during the hydrothermal aging treatment. It is known that copper species can be changed during the hydrothermal aging treatment process either by agglomerating into CuO_x clusters or by reacting with Al to form $CuAlO_x$ moieties. From the curve-fitting

results of Cu $2p_{3/2}$ XPS spectra (Figure 7 and Table 2) and H_2 consumption analysis (Figure 8, Figure 9 and Table 3), one can see the changes of the bulk and surface Cu species after the hydrothermal aging treatment. For the Ce-, Gd-, La- or Nd-doped Cu-SAPO-18 sample, the Cu species were still mainly isolated, while for the Ho-, Tb- or Lu-doped Cu-SAPO-18 sample, the content of the isolated Cu^{2+} species decreased considerably. From the Cu 2p3/2 XPS and H_2-TPR results, it is found that Ce, Gd, La or Nd promoted the reduction of the Cu^{2+} species before or after the hydrothermal aging treatment. Therefore, the doping of Ce, Gd, La or Nd improved the hydrothermal stability of the Cu-SAPO-18 sample. Especially, after Ce doping, the catalyst possessed the greatest resistance to hydrothermal aging treatment.

4.3 Effect of Lanthanide Doping on NH_3-SCR

The NH_3-SCR reaction over the Cu/zeolite catalysts has been extensively investigated. According to the results presented above, the co-doping of Cu and M could affect the NH_3-SCR performance. Introduction of a lanthanide element to Cu-SAPO-18 might influence the interaction between the Cu^{2+} and AEI framework and accordingly the relative positions of the Cu^{2+} species within the 8MRs cage. On the other hand, lanthanide introduction could affect the accessibility of the reactants to the Cu^{2+} species and thereby the interaction between the isolated Cu^{2+} species and the reactants.

It is assumed that the reactants (NO, NH_3, and O_2) pass through the catalyst bed by a plus flow and the reaction products are removed together in the catalyst channel. Due to the low concentrations of the reactants (NO and NH_3) in the NH_3-SCR reaction,

the change in temperature induced by the heat of the chemical reactions can be neglected. That is to say, the isothermal condition is considered in the catalytic system. The NO reaction rate as a function of reactant concentrations can be defined below [42,43]:

$$r_{[NO]} = -kC_{NO}{}^{\alpha}C_{NH_3}{}^{\beta}C_{O_2}{}^{\gamma} \quad (1)$$

where the $r_{[NO]}$ represents the NH_3-SCR reaction rate, k is the apparent rate constant, and the α, β, and γ are the reaction orders with respect to NO, NH_3, and O_2 concentrations, respectively.

Over the Cu-AEI catalyst, the order (α) with respect to NO concentration for the NH_3-SCR reaction is usually set to 1. Gao et al. studied the power-law dependence in NH_3 partial pressure over the CuSSZ-13 catalyst at the order (β) with respect to NH_3 of 0 [41]. The SAPO-18 was a kind of zeolite similar to the SSZ-13 structure. When the NH_3/NO molar ratio was higher than or equal to 1, the order (β) with respect to NH_3 concentration for the NH_3-SCR reaction was close to zero. Since O_2 was in considerable excess for the NH_3-SCR reaction, the influence of O_2 on the SCR reaction could be omitted. Thereby, the order (γ) with respect to O_2 concentration for the NH_3-SCR reaction was also zero. Therefore, the orders with respect to NO, NH_3, and O_2 concentrations are approximately 1, 0, and 0, respectively. Eq. (1) could be simplified as a first-order reaction:

$$r_{[NO]} = -kC_{NO} \quad (2)$$

The Arrhenius equation is:

$$k = Ae^{-E_a/RT} \quad (3)$$

where A is the pre-exponential factor and E_a is the apparent activation energy.

According to the above SCR kinetics results (Figures 2 and 3), the activation energies of the M-Cu-SAPO-18 samples were similar to that of the Cu-SAPO-18 sample, demonstrating that the NH_3-SCR reaction was mainly carried out in the Cu-ion sites. In other words, Cu ions were the catalytic active centers in all of the samples, and the significantly higher SCR rate over the Ce-Cu-SAPO-18 sample was caused by the variation in pre-exponential factor. For instance, the position of the isolated Cu^{2+} species could be changed through migration in the Ce-doped Cu-SAPO-18 sample, which accounted for the change in pre-exponential factor of Eq. (3). Therefore, it is clear that the catalytic performance was improved after the doping of Ce to Cu-SAPO-18.

From Figures 1 and 2, it can be seen that all of the samples showed different extents of decline in catalytic activity after the hydrothermal aging treatment. For the hydrothermally aged samples, the isolated Cu^{2+} species might migrate to the positions of the negative framework charge centers, as compared with the fresh samples. This would weaken the accessibility of the reactants to the active centers and increase the barrier to the reaction, thus reasonably explaining the reason why the catalytic activity decreased over the hydrothermally aged samples. The activation energies obtained over the hydrothermally aged samples were calculated according to Eqs. (2) and (3). The activation energy obtained over the Ce-Cu-SAPO-18-aged sample was ca. 31.1 kJ/mol, which was slightly different from that obtained over the fresh sample. The activation energy decreased in the sequence of Tb-Cu-SAPO-18-aged (45.1 kJ/mol) > Cu-SAPO-

18-aged (40.6 kJ/mol) > Gd-Cu-SAPO-18-aged (38.4 kJ/mol) > La-Cu-SAPO-18-aged (38.1 kJ/mol) > Lu-Cu-SAPO-18-aged (37.6 kJ/mol) > Ho-Cu-SAPO-18-aged (36.3 kJ/mol) > Nd-Cu-SAPO-18-aged (35.4 kJ/mol) > Ce-Cu-SAPO-18-aged (31.1 kJ/mol). The Tb-Cu-SAPO-18-aged sample showed a more significant drop in SCR reaction rate and the activation energy also increased obviously from 30.5 kJ/mol obtained over Tb-Cu-SAPO-18 to 45.1 kJ/mol obtained over Tb-Cu-SAPO-18-aged, which was consistent with NO conversion in the NH_3-SCR reaction. After Cu and M (except Ce) were doped, the amount of the isolated Cu^{2+} species decreased and the redox ability of the samples also decreased after the hydrothermal aging treatment. From the XPS and H_2-TPR results, the Ce and Cu ions in the Ce-Cu-SAPO-18-aged sample interacted more weakly with the framework at low temperatures, showing an enhancement in activity and the still residing of the Cu^{2+} species in the energetically most favorable sites after the hydrothermal aging treatment. Therefore, the Ce-Cu-SAPO-18 sample possessed the best hydrothermal stability.

4.4 Applicability for Lanthanide Doping Cu-SAPO-18 SCR Catalysts

The dispersion state of copper species was closely related to the temperature window of NH_3-SCR reaction over the Cu-AEI catalyst, and also affected the hydrothermal stability of the catalyst. The solution to this problem was to change the dispersion state of the Cu species and the interaction between the Cu and framework. Doping of lanthanide elements may overcome the above shortcomings. In the lanthanide-doped sample, the amount of the isolated Cu^{2+} species increased and the Cu ions interacted with the framework more weakly, leading to an enhancement in catalytic

activity and the residing of the isolated Cu^{2+} species in the energetically most favorable sites during the hydrothermal aging treatment process. Therefore, high SCR activity was maintained and the AEI structure was stabilized. As discussed above, Ce doping gave rise to the best catalytic activity (Figure 1) and broadened the reaction temperature window. In addition, the Ce-Cu-SAPO-18 sample could still maintain high catalytic activity after the hydrothermal aging treatment, but the other lanthanide doping seemed to be less able to effectively promote the improvements in catalytic activity and hydrothermal stability.

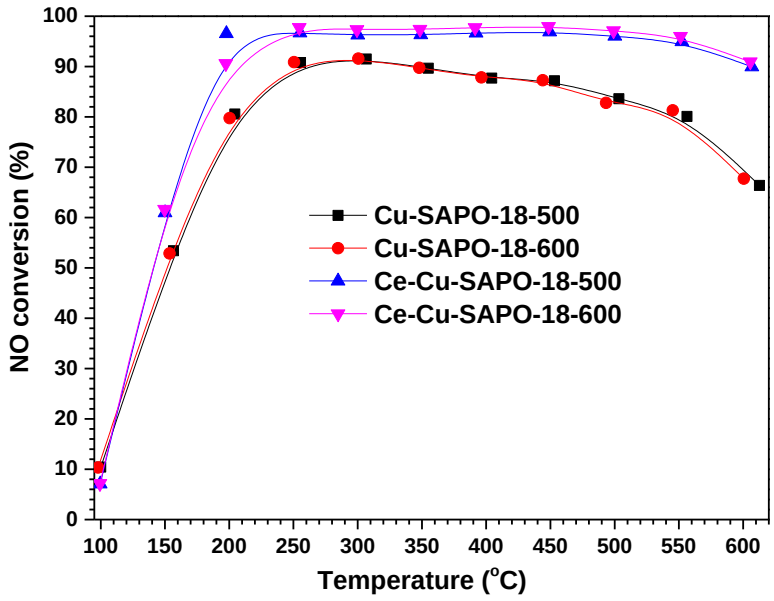

Fig. S1. NO conversion of the Cu-SAPO-18 and Ce-Cu-SAPO-18 catalysts at different calcination temperatures (500 and 600 °C). The reactant feed composition: 500 ppm NO + 500 ppm NH_3 + 14 vol% O_2 + 5 vol% H_2O + N_2 (balance); GHSV = 130,000 h^{-1}.

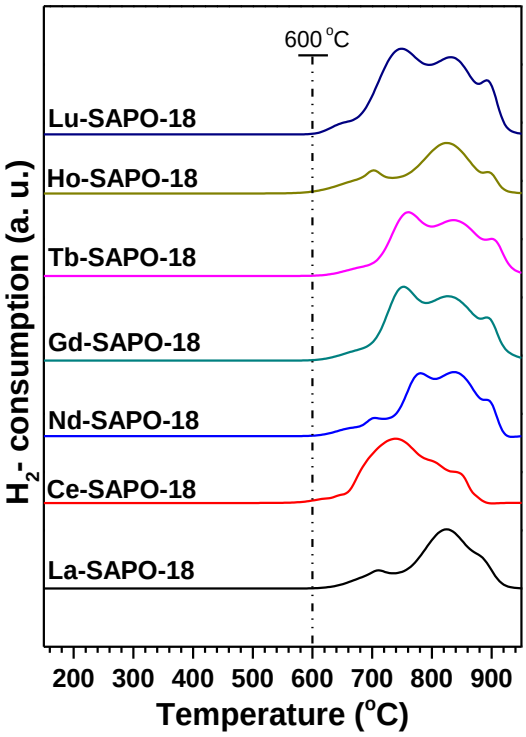

Fig. S2. H_2-TPR profiles of the M-Cu-SAPO-18 samples (M = La, Ce, Nd, Gd, Tb, Ho, and Lu).